PCCP

Accepted Manuscript

ROYAL SOCIETY OF CHEMISTRY

www.rsc.org/pccp

Journal Name

ARTICLE TYPE

Cite this: DOI: 10.1039/xxxxxxxxxx

Time scale of dynamic heterogeneity in model ionic liquids and its relation to static length scale and charge distribution†

Sang-Won Park, Soree Kim, and YounJoon Jung*

Received Date
Accepted Date

DOI: 10.1039/xxxxxxxxxx

www.rsc.org/journalname

We study how dynamic heterogeneity in ionic liquids is affected by the length scale of structural relaxation and the ionic charge distribution by the molecular dynamics simulations performed on two differently charged models of ionic liquid and their uncharged counterpart. In one model of ionic liquid, the charge distribution in the cation is asymmetric, and in the other it is symmetric, while their neutral counterpart has no charge with the ions. It is found that all the models display heterogeneous dynamics, exhibiting subdiffusive dynamics and nonexponential decay of structural relaxation. We investigate the lifetime of dynamic heterogeneity, τ_{dh}, in these systems by calculating the three-time correlation functions to find that τ_{dh} has in general a power-law behavior with respect to the structural relaxation time, τ_α: $\tau_{dh} \propto \tau_\alpha^{\zeta_{dh}}$. Although the dynamics of the asymmetric-charge model is seemingly more heterogeneous than that of the symmetric-charge model, the exponent is found to be similar, $\zeta_{dh} \approx 1.2$ for all the models studied in this work. The same scaling relation is found regardless of interactions, *i.e.*, with or without Coulomb interaction, and it holds even when the length scale of structural relaxation is long enough to become the Fickian diffusion. This fact indicates τ_{dh} is a distinctive time scale from τ_α, and the dynamic heterogeneity is mainly affected by the short-range interaction and the molecular structure.

1 Introduction

Ionic liquids (ILs) are a new class of organic molecules that are composed of cations and anions and usually have melting points near room temperature. Currently ILs are attracting significant interest both from industry and academia due to their unique properties and possible applications in diverse areas. Because the components of ILs can be varied in a great number of combinations, one can in principle design appropriate IL solvents for specific purposes in applications. Due to their high polarity ILs are also able to dissolve a wide range of different molecules. Because ILs have a negligible vapor pressure due to their strong Coulomb attraction, they are considered to be "green" alternatives to typical volatile, inflammable and toxic organic solvents.[1]

Most ILs consist of bulky, asymmetric cations and small, symmetric anions. It has been reported that IL is much more viscous than its counterpart of neutral binary mixture,[2,3] and it becomes less viscous as the charge is distributed more homogeneously on the molecule, mostly on a cation,[4–7] leading us to expect that Coulomb interaction may influence their glassy dynamics, and that the charge distribution of an ionic component can significantly affect dynamic properties of the IL. According to simulation[3,7–22] and experimental[2,23,24] studies, ILs exhibit slow dynamical behavior that are typically characterized by subdiffusivity and nonexponential relaxation as in glass forming liquids.

The overall nonexponential dynamics in glass forming liquids may be ascribed to either homogeneously nonexponential relaxation behavior or the superposition of exponential relaxations with different relaxation times in two limiting cases. Extensive studies performed so far point toward the picture that the latter, heterogeneous dynamics, is the case with ILs,[3,7–19] which is in accordance with previous studies on other glass forming liquids,[25] such as supercooled liquids,[26–52] polymer melts,[53–58] and colloids.[59–61] Time and length scale of dynamic heterogeneity is important for obtaining microscopic understanding of dynamical behavior of liquids, and they have been subject to intensive investigations, recently, in supercooled liq-

* *Department of Chemistry, Seoul National University, Seoul 08826, Korea. E-mail: yjjung@snu.ac.kr*

† Electronic Supplementary Information (ESI) available: [Detailed method of MSAD calculation and dependence of the time interval on it]. See DOI: 10.1039/b000000x/

uids[31–49,62] and polymer melts,[55–58] but very few in ILs.[15] The dynamic length scale adapted from the framework of conventional critical phenomena has been widely used in studies on dynamic heterogeneity.[15,25,32–39,62] The importance of time scale of dynamic heterogeneity in glassy dynamics and in glass transition also has been shown in both numerical and experimental research mainly from its phenomenological approach.[31,38–47,55–58] Despite such interest, the dynamic length and time scales of ILs and the relation between them have not been thoroughly understood.

Coarse-graining ILs is a very common strategy in reducing the computation time because performing simulations for ILs is very time-demanding due to not only their intrinsically slow dynamics but also Ewald summation method, which is inevitable for calculating long range interactions. In an effort to make the simulations of ILs efficient, various levels of coarse-grained models have been developed for studying their structural and dynamic properties.[3,7–11,63] Since our purpose of this study is to characterize the qualitative behavior of dynamic heterogeneity and to find the origin of it in ILs in molecular level, a simplest possible model maintaining glassy dynamics is the most suitable for this study.

For that purpose, we utilize two different, simple models of ILs introduced by a previous study.[7] One model mimics the case of symmetrical charge distribution in cation molecules, while the other asymmetric one in cations. In both models, asymmetry in the cation shape is introduced to prevent the ILs from crystallizing. We also explore the neutral model with the same molecular shape. With these models, we study the dynamic properties of IL systems via performing molecular dynamics simulations. In particular, we focus on the issue of the correlation between the local charge distribution of cations and the dynamic heterogeneity of ILs by investigating the lifetimes of dynamic heterogeneity by calculating their three-time correlation functions (3TCFs) in these systems.

The validity of the 3TCF as a quantity measuring the dynamic heterogeneity is examined from the relation between the time scale of the 3TCFs and that of the two-point correlation functions, such as the structural relaxation and the relaxation of rotational motion. Moreover, the dependence of the dynamic heterogeneity time scale on the length scale of the structural relaxation time is explored. We find that the lifetime of the 3TCFs is the distinct time scale of dynamic heterogeneity, and we believe that this work is the first that has investigated the relation between the time scale of dynamic heterogeneity and the length scale of the structural relaxation in ILs.

The remainder of this paper is organized as follows. Section II is devoted to model descriptions and simulation methods. In Section III, we present our main results on the lifetime of dynamic heterogeneity in the model IL systems, and discuss our findings. Finally, we summarize the results and conclude in Section IV.

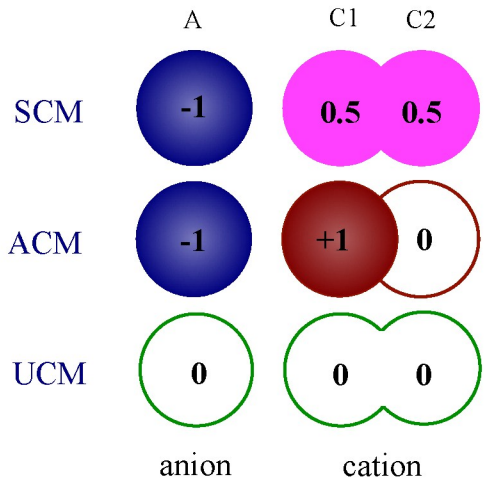

Fig. 1 Schematic representation of the three models: symmetric-charge model, or SCM (top) and asymmetric-charge model, or ACM (middle) are representing ILs, and uncharged model, or UCM (bottom) is uncharged glass forming liquids with the same molecular structure. In SCM two spherical cationic components share the positive charge equally for each having 0.5 e, and in ACM only one sphere (C1) has the positive charge, 1.0 e. Their uncharged counterpart UCM, however, does not have any charged components.

2 Models and Simulation Methods

Most ILs consist of bulky, asymmetric cations and small, symmetric anions. Preferred choices for cations include 1-alkyl-3-methylimidazolium, pyridinium, pyrrolidinium, tetraalkylammonium, and tetraalkylphosphonium ions, and for anions tetrafluoroborate (BF_4), hexafluorophosphate (PF_6), trifluoromethanesulfonate, and bis(trifluoromethylsulfonyl)imide ions. Although it is not possible that the ions take different charge distribution with the molecular geometry fixed in real experiments, it has been reported that the liquid becomes less viscous as the charge is distributed more homogeneously on the molecule from simulation studies,[5–7] where it is expected that the charge distribution of an ionic component can significantly affect dynamic properties of the ILs. We thus choose two extreme cases of charge distribution: symmetric and asymmetric.

Our key purpose is to focus on the issue of charge distributions of IL molecules on their dynamical properties and to find their qualitative trends, or scaling relations, not to reproduce quantitatively exact values to real systems. We are exempted from realizing molecular details, and in order to make the simulation efficient we employ two simple, coarse-grained models of ILs that were previously introduced in Ref. [7] and an uncharged model as a counterpart of the two IL models. Their schematic molecular structures are shown in Fig. 1. Because coarse-graining itself is simplifying the molecular details, including charge fluctuation in the molecules is not a clever tactics, we fix the partial charges neglecting the polarization effect.

We choose a two-site model for the cation since it mimics an IL system better than a single-site cation model, and it simplifies more than preexisting three-site and four-site coarse-grained models.[3,8,11] Less symmetric molecular structure of this model not only prevents the crystallization that would occur more easily in a single-site model, but it also enables us to investigate rotational dynamics, thus we can investigate translational and rotational glassy dynamics with this model. Its simplicity relative to other coarse-grained models enables us to simulate for a longer time.

In both models of ILs, the anion is represented by a single spherical particle (A) of mass, m, 200 amu, and the cation by two spherical particles (C1 and C2) connected through a rigid bond, where the mass of each particle is set to be 100 amu so that the total mass of cation is the same as that of anion. In the symmetrically charged model (SCM) the two spheres have the same charges ($+0.5\ e$, where e is the elementary charge), while in the asymmetric-charge model (ACM) one (C1) of the two spherical particles has $+1.0\ e$ and the other (C2) zero. The anion has $-1.0\ e$ for both models. The uncharged model (UCM) has the same molecular structure as the IL models except that all the components do not have charges, but we stick to "cation" and "anion" for big and small species of UCM for the sake of convenience. On top of the Coulomb interactions between charged particles, they also interact with Lennard-Jones potential with each other in all models. We could find no crystallization within the simulation times at each temperature, except that ACM crystallizes at $T = 1.73$, right below the lowest temperature studied for ACM.

We perform classical molecular dynamics (MD) simulation using the above models. All the MD trajectories are obtained from GROMACS 4.5 MD package program.[64] The total potential energy is given by the sum of the pairwise interactions of two different types: the repulsive Lennard-Jones (LJ) potential and the Coulomb potential,

$$U_{\text{total}} = \sum_{<i,j>} \left\{ U_{\text{LJ}}(r_{ij}) + U_{\text{Coulomb}}(r_{ij}) \right\}, \qquad (1)$$

where $< i, j >$ indicates that the sum is performed over the i-th and j-th coarse-grained particles, and

$$U_{\text{LJ}}(r_{ij}) = 4\varepsilon_{ij} \left[\left(\frac{\sigma_{ij}}{r_{ij}} \right)^{12} - \left(\frac{\sigma_{ij}}{r_{ij}} \right)^{6} + \frac{1}{4} \right] H(r_{\text{cut}} - r_{ij}) \qquad (2)$$

and

$$U_{\text{Coulomb}}(r_{ij}) = \frac{1}{4\pi\varepsilon_0} \frac{q_i q_j e^2}{r_{ij}}. \qquad (3)$$

Here, $H(r_{\text{cut}} - r_{ij})$ is the Heaviside step function, where the cutoff distance is set to be $r_{\text{cut}} = 2^{1/6}\sigma_{ij}$ in order to make the Lennard-Jones potential purely repulsive by adopting the Weeks-Chandler-Andersen (WCA) potential.[65] In all the models $\varepsilon_{ij} = \varepsilon = 2$ kJ/mol and $\sigma_{ij} = \sigma = 0.5$ nm for all i, j-pairs, and the bond between the two spheres is rigid with a bond distance $d = 0.8\sigma$. q_i is the partial charge of i species (Fig. 1). With the unit length, energy, and mass, σ, ε, and m, respectively, the other units are converted by the following relations: unit time, $t_0 = (m\sigma^2/\varepsilon)^{1/2} = 5$ ps, unit temperature, $T_0 = \varepsilon/k_{\text{B}} = 240.5$ K, unit charge, $q_0 = (4\pi\varepsilon_0\sigma\varepsilon)^{1/2} = 0.08484\ e$, and unit pressure, $P_0 = 262.2$ atm.

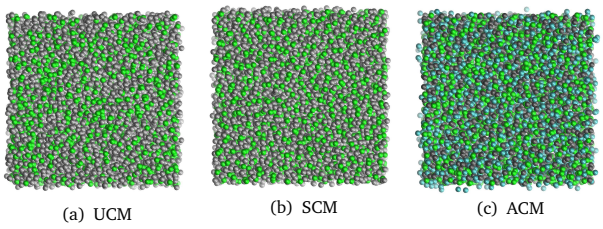

(a) UCM (b) SCM (c) ACM

Fig. 2 Snapshots of UCM (a), SCM (b), and ACM (c) at the lowest temperature of each model. Colored (green or cyan) and gray particles respectively denote cations and anions. For ACM we distinguish the uncharged (0 e) component from the charged (+1.0 e) one with cyan and green. Compared to UCM, IL models show alternating structure preventing the same species from being positioned at the nearest neighbor.

The model parameters used in this study are comparable to ones from previous simulation studies on ILs, ranging from 1-ethyl-3-methylimidazolium (EMIM) to 1-butyl-3-methylimidazolium (BMIM) for the cation and BF_4 or PF_6 for the anion.[3,11,22,66] With those parameters SCM remains as liquid state at room temperature. As the purpose of this study is focused on finding out general trends in dynamic properties of ILs with respect to the charge distribution on the molecules, these models with plausible parameters are thought to be simplest model systems to investigate glassy dynamics of ILs.

All simulations are performed at the fixed reduced density $\rho^* = \rho\sigma^3 = 0.716$, where $\rho = (N_+ + N_-)/V$ is the total number density with N_+ and N_- being the number of cations and anions, respectively. In our simulations we use a total of 4096 ions, *i.e.*, 2048 pairs of IL molecules in our simulations, $N_{\text{pair}} = N_+ = N_- = 2048$ contained in the cubic simulation box of a linear dimension of $L = 17.88$, and a periodic boundary condition is applied. The box size is determined by equilibrating with NPT simulation at $P = 10$ and $T = 1$, for SCM, and we fix all the simulation boxes of all models at all temperatures with this value. Even if the systems are in high pressure condition and have different pressures by fixing the volume with the same value, the qualitative trends of dynamics should be little affected.[67] We also checked our results with different size of systems such as $N_{\text{pair}} = 512$, 1024, 2048, and 4096 to find no significant finite size effect with $N_{\text{pair}} = 2048$ on the structural relaxation times. We employ the NVT ensemble combined with the Nosé-Hoover thermostat in our simulations. The time step is chosen as $\delta t = 0.0004$, and the relaxation time constant for the thermostat as $200\delta t$. Both the LJ potential and the Coulomb potential are truncated at 5. For calculating long-range electrostatic interaction PME is used. The Verlet leapfrog algorithm is employed to integrate the equations of motion. Each system is first equilibrated from a higher temperature until the

energy fluctuation is found to be stable for around its structural relaxation time, τ_α, and then a production run is carried out from this equilibrated configuration to obtain a sample trajectory, whose total run time is about 40 times of the τ_α at each temperature. At all temperatures studied in this work, 10 independent trajectories are produced, and structural and dynamic properties are averaged over those trajectories.

3 Results and Discussion

3.1 Liquid structure

The structure of the models is firstly investigated by calculating the radial distribution functions (RDFs), $g(r)$, for all the models, where r is the distance between the centers of mass of the ions. While we have calculated RDFs at all the temperatures studied in this paper, those at the highest ($T = 6$ for both IL models, and 1.14 for UCM) and the lowest ($T = 1.04$, 1.75, and 0.29 for SCM, ACM, and UCM, respectively) temperatures are shown in Fig. 3.

Firstly, we note that all the models exhibit typical structures of amorphous liquid, and they do not show any sign of crystallizations at all temperatures we have studied. The first peak of RDF determines the closest length scale, which is 1 for all the species in UCM, the same as the value of σ of our models. In the ILs' RDFs the first peaks between the equally charged species ($\sigma_+ = 1.46$ and $\sigma_- = 1.5$ for SCM, and 1.54 and 1.32 for ACM) appear at a distance longer than σ due to the repulsive interactions while those between the oppositely charged species ($\sigma_\pm = 0.92$ and 0.94 for SCM and ACM, respectively) at a distance shorter than σ due to attractive interactions. The difference between $\sigma_\pm$ and σ_+ or σ_- is consistent to the alternating structure of the IL models found in Fig. 2.

The shapes of the RDFs of both IL models are generally similar to each other. At the high temperature, $T = 6$, the structures of RDF are very similar in both cases while the peak splits in anion-anion RDF for ACM. There are notable differences, especially at a lower temperature. For example, in the case of anion-anion RDF of ACM at $T = 1.75$, there is a distinct second peak located at $r \approx 1.8$ while it is weakened in SCM. Also, the cation-cation RDF appears more broader in ACM than in SCM. The fact that positive charges are distributed more asymmetrically in ACM than in SCM makes it possible for cations to have more local arrangements, which yields a broader first peak in ACM. The environments where a particle is positioned are different for both models. SCM provides less complex environment due to symmetry in the charge distribution of the cation despite the geometrical asymmetry while for ACM an anion forms a strong ion pair preferentially to one (C1) of the two cationic components, which is a feasible motive inducing structural heterogeneity, and this may affect dynamic properties. We will discuss this point later in this paper.

3.2 Dynamic properties

A two-point correlation function characterizing structural relaxation is the self-intermediate scattering function (ISF),

$$F_s(q,t) = \left\langle \frac{1}{N}\sum_{j=1}^{N} \exp\left[-i\mathbf{q}\cdot\Delta\mathbf{r}_j(t_0,t_0+t)\right]\right\rangle = \left\langle \frac{1}{N}\sum_{j=1}^{N} \cos\left[\mathbf{q}\cdot\Delta\mathbf{r}_j(t_0,t_0+t)\right]\right\rangle, \quad (4)$$

where $\Delta\mathbf{r}_j(t_0,t_0+t) = \mathbf{r}_j(t_0+t) - \mathbf{r}_j(t_0)$, $\mathbf{r}_j(t')$ is the position vector of the center of mass of the j ion at time t', and $\langle\cdots\rangle$ denotes average over the reference time t_0. We take $q = q^* = |\mathbf{q}^*| = 2\pi/\sigma_\pm$, where $\sigma_\pm$ is the distance at the first peak of the radial distribution function, $g_{CA}(r)$, of the cation-anion pair, and it is set to be the shortest length scale, the distance between the cation and the anion, $q^* = 6.83$, 6.68, and 6.28 for SCM, ACM, and UCM, respectively. We compare the time scales of $F_s(q^*,t)$ and $F_s(q_0,t)$, where the latter is more conventional.[11,51] q_0 for the cation and the anion respectively are the maximum positions of the static structure factors, $S_{CC}(q)$ and $S_{AA}(q)$, calculated by Fourier transform of $g_{CC}(r)$ and $g_{AA}(r)$, and the values are $q_0 = 4.83(4.83)$, 4.99(5.07), and 4.69(4.69) for cation(anion) of SCM, ACM, and UCM, respectively. We will compare the results with two more different q values: π and $q_0/2$. For the wave vector, $\mathbf{q}$, being isotropic, we calculate $F_s(q,t)$ in terms of cosine as in Eq. (4) instead of exponential for dynamic filtering discussed later in Section 3.3. The α-relaxation time, $\tau_\alpha(q)$, is defined such that $F_s(q,t=\tau_\alpha) = 1/e$.

The rotational dynamics is also taken into account in order to find its relation to the translational dynamics. The correlation function characterizing rotational dynamics is defined as

$$C_l(t) = \left\langle \frac{1}{N}\sum_{j=1}^{N} P_l(\hat{\mathbf{u}}_j(t)\cdot\hat{\mathbf{u}}_j(0))\right\rangle, \quad (5)$$

where P_l is Legendre polynomial of order l, and $\hat{\mathbf{u}}_j(t')$ is the orientation vector of the j-th cation at time t'. The rotational relaxation time, $\tau_R^{(l)}$, is defined such that $C_l(t=\tau_R^{(l)}) = 1/e$, and we take $l = 2$ for its experimental significance.[26,59]

Comparing the length scales, q_0 and q^*, we find that with q^* the $F_s(q,t)$ and $C_2(t)$ of the cation show the more similar decays, and the two time scales are comparable and coupled: $\tau_R^{(2)} \propto \tau_\alpha(q^*)$, shown in Fig. 6(a). $F_s(q^*,t)$ and $C_2(t)$ at the selected temperatures for the cation (full line) and the anion (dashed line) are shown in Fig. 4. Both correlation functions at high temperatures show single decay while at low temperatures the process splits into two steps and the long time decay is nonexponential, and this nonexponentiality becomes greater as temperature decreases. According to experimental[40,41,55] and simulation studies[53,54] on glass forming liquids, this nonexponential decay of translational dynamics is attributed to heterogeneous dynamics.

τ_α of ACM increases more steeply than for SCM as temperature decreases (Fig. 6(b)). All the models show Arrhenius

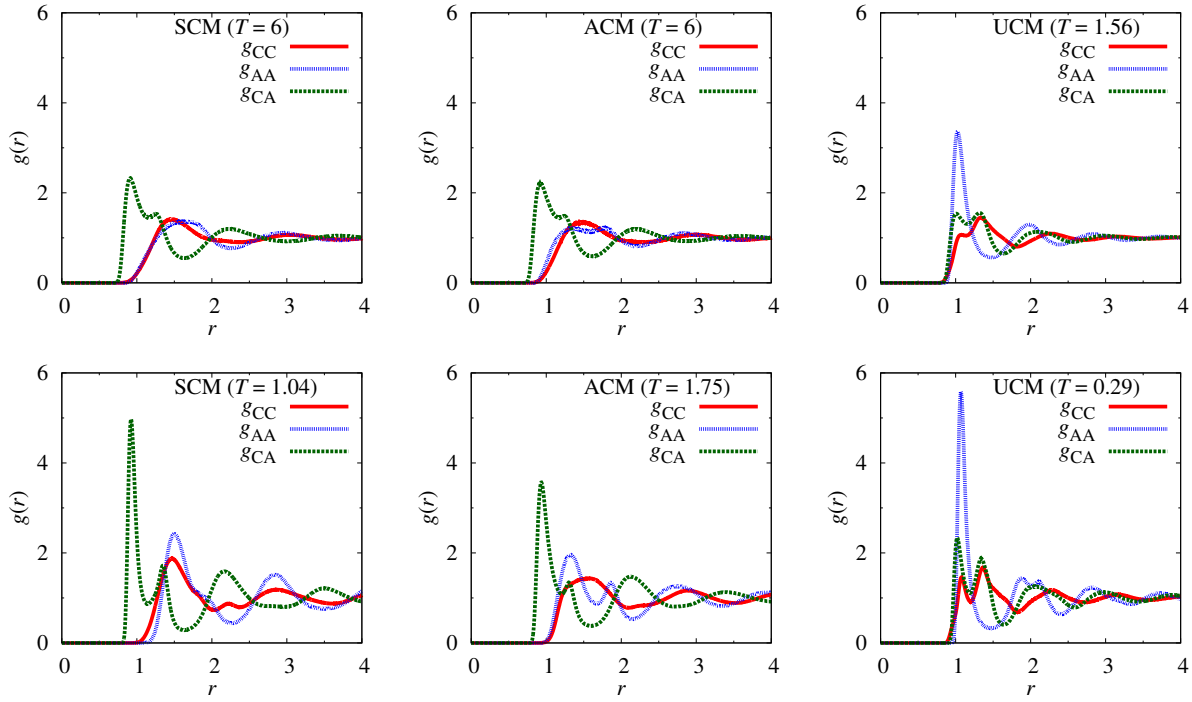

Fig. 3 Center of mass radial distribution functions, RDFs, at the highest temperatures (top) and the lowest temperatures (bottom) of SCM, ACM, and UCM, respectively. g_{CC}, g_{AA}, and g_{CA} are the RDFs of cation-cation, anion-anion, and cation-anion pairs, respectively. Both IL models have similar liquid structures at high temperature (left and center of top panels). Unlike UCM IL models show alternating structure: the first peak of g_{CA} appears closer than those of g_{CC} and g_{AA}. (See Fig. 2)

behavior at high temperature, and they start to show super-Arrhenius behavior at T <2.5, 3.6, and 0.6 for SCM, ACM, and UCM, respectively, $\tau \propto \exp[A/T^{\nu}]$, where $\nu > 1$, thus fragile. Two major fitting laws of the super-Arrhenius behavior of fragile liquids are Vogel-Fulcher-Tamman (VFT) and parabolic[68,69] forms, which have different origin of fragility: whether there is finite temperature glass transition (the former) or there is no such transition (the latter). Both are fitted well (Fig. 6(c)), however, in the temperature range of our simulations. Since ACM is easy to crystallize below the lowest temperature in this work, the range is quite narrow. SCM and UCM are not thought to be in deeply supercooled regime that in this temperature range we cannot discuss the validity of the two explanations. From its appearance perspective ACM seems the most fragile.

Another way of obtaining the dynamical properties is through the mean squared displacement (MSD) defined as

$$\left\langle \Delta \mathbf{r}^2(t) \right\rangle = \left\langle \frac{1}{N} \sum_{j=1}^{N} |\Delta \mathbf{r}_j(t_0, t_0+t)|^2 \right\rangle, \qquad (6)$$

and the mean squared angular displacement (MSAD)[a] as

$$\left\langle \Delta \boldsymbol{\phi}^2(t) \right\rangle = \left\langle \frac{1}{N} \sum_{j=1}^{N} |\Delta \boldsymbol{\phi}_j(t_0, t_0+t)|^2 \right\rangle, \qquad (7)$$

where

$$\Delta \boldsymbol{\phi}_j(t', t'') = \int_{t'}^{t''} dt \boldsymbol{\omega}_j(t), \qquad (8)$$

and $\boldsymbol{\omega}_j(t)$ is the angular velocity of the j-th cation at time t.[50–52,61] The translational diffusion constant is obtained from the Einstein relation,[70] $D = \lim_{t\to\infty} \left\langle \Delta \mathbf{r}^2(t) \right\rangle / 6t$, and we fit the MSDs at the long time regime, *i.e.*, the time scale at which $\left\langle \Delta \mathbf{r}^2(t) \right\rangle \propto t$. The rotational diffusion constant, $D_R = \lim_{t\to\infty} \left\langle \Delta \boldsymbol{\phi}^2(t) \right\rangle / 4t$, is obtained from the MSADs. The MSDs for the cation and the anion and the MSADs for the cation are calculated for several temperatures ranging from $T = 1.04$ to 6 for SCM, $T = 1.75$ to 6 for ACM, and $T = 0.29$ to 1.56 for UCM as presented in Fig. 5. At low temperature the time scales for all the systems can be separated into three distinct time regimes: the ballistic regime at short time ($\left\langle \Delta \mathbf{r}^2(t) \right\rangle \propto t^2$), the diffusive regime at long time ($\propto t$), and the subdiffusive regime at intermediate time ($\propto t^{\alpha}, 0 < \alpha < 1$). All the models show sub-

[a] Detailed method of MSAD calculation and dependence of the time interval on it is described in ESI.

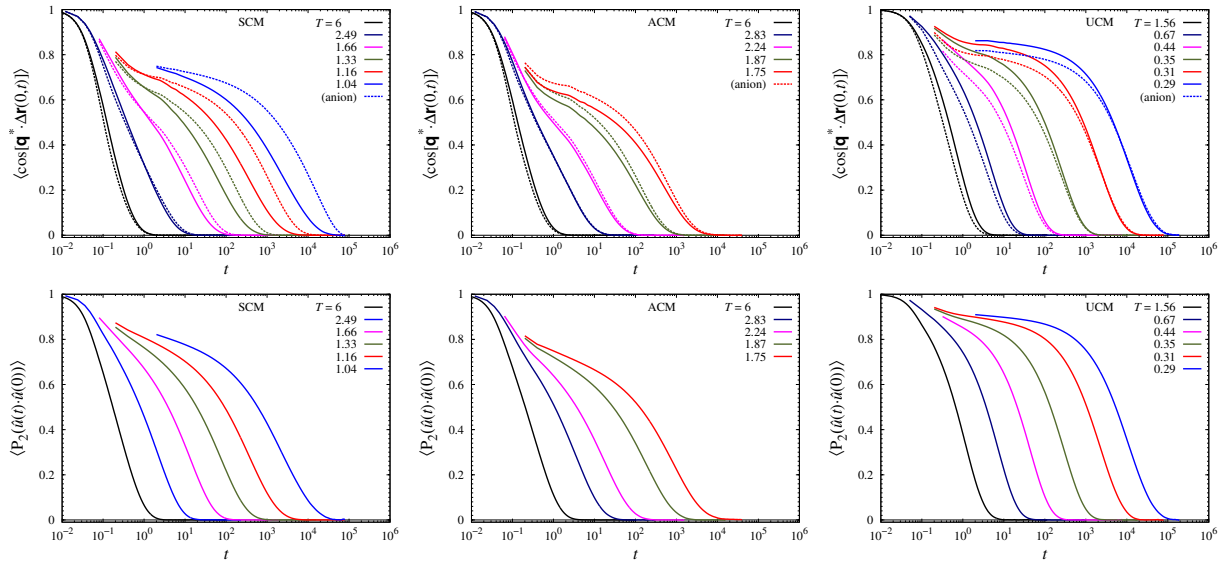

Fig. 4 Intermediate scattering function at the selected temperatures for the cation (full line) and the anion (dashed line) at the length scale, $q = q^* = 2\pi/\sigma_{\pm}$, where $\sigma_{\pm}$ is the peak position of g_{CA} (Fig. 3), and the values are 0.92, 0.94, and 1, respectively in SCM (left) ACM (center), and UCM (right). Comparing the length scales with $q = q_0$ and q^*, we find that at this length scale the $F_s(q^*,t)$ (top) and $C_2(t)$ (bottom) show the most similar decays and the two time scales, $\tau_\alpha(q^*)$ and $\tau_R^{(2)}$, of the cation are comparable. The ISF at the high temperature shows single decay while at low temperatures the process at long time decays nonexponential, and this nonexponentiality becomes greater as temperature decreases.

diffusive dynamics at the intermediate time scale at low temperature, and this time regime becomes longer as temperature decreases. The rotational diffusion, however, is quite different from the translational one in that the subdiffusive regime is much shorter for the former at low temperature. The time scales represented by ISFs are comparable to those by MSDs (Fig. 5), in that the process at the short time decay falls into the ballistic regime, the long relaxation time corresponds to the diffusive regime, and the plateau at the intermediate time scale is attributed to the subdiffusive motion.

This subdiffusive behavior is one of distinct properties of glass formers, and has been perceived as being ascribed to a multiple step process. When a particle is trapped in a cage by other particles, it takes time to escape, which causes the subdiffusive dynamics.[16,17,19,22] According to simulation studies on IL systems,[17,18,53] the dynamics becomes heterogeneous at the time scale a particle is about to escape the cage. From this context one may expect that the rotational motion shows less heterogeneous dynamics.

It is obvious that the Coulomb interaction makes the dynamics slower comparing the ISFs and the MSDs knowing from the temperature range of IL models and UCM. Comparing the translational motion of the two IL models, SCM is faster than that in ACM at the same temperatures. Since the masses and the molecular geometry of each species for both models are set to be the same, the difference of the translational motion is mainly due to the difference in the molecular charge distribution in a cation. It is notable that these models show more consistent results than the one-site models,[6] where the one with the charge off-centered produces faster dynamics than the one with the charge at the center, but in the experiment study the dynamics of ILs having cations with charge delocalized, such as BMIM and *N*-butyl-*N*-methylpyrrolidinium (P14), are greater than those in systems with charge more off-centered, such as *N*-hexyl-*N*,*N*,*N*-trimethylammonium (N6111).[5]

Comparing the structural relaxation time of each ion species, the anion, having the smaller size than the cation, relaxes faster than the latter at high temperature of all models (see Fig. 4). With cooling down the anion relaxes more slowly than the cation for IL models, and the relaxation of both species for UCM collapses. The faster relaxation of the cation in ILs is consistent to previous studies.[11,13,20] Since the geometry and all the other parameters are the same for all the models, this discrepancy between the ion species of ILs is attributed to the charge distribution.

On the other hand, the MSD in ACM shows quite a different trend from the ISF. The diffusive motion of the anion is faster than the cation, and the reverted trend at the subdiffusive regime occurs only at low temperature. Since in typical ILs the cation has greater D than the anion,[4,11] the ACM is considered as an extreme case in charge distribution.

The Stokes-Einstein (SE) relation, $D \sim k_B T/\eta$, where η is shear viscosity, is valid in wide range of liquids, but it breaks down in glass forming liquids near glass transition temperature, and it has been adopted as an evidence showing glassy dynamics. Two alternate relations have been adopted in studies on the violation of the SE relation in order to reduce computation time requiring for calculating the shear viscosity. In one

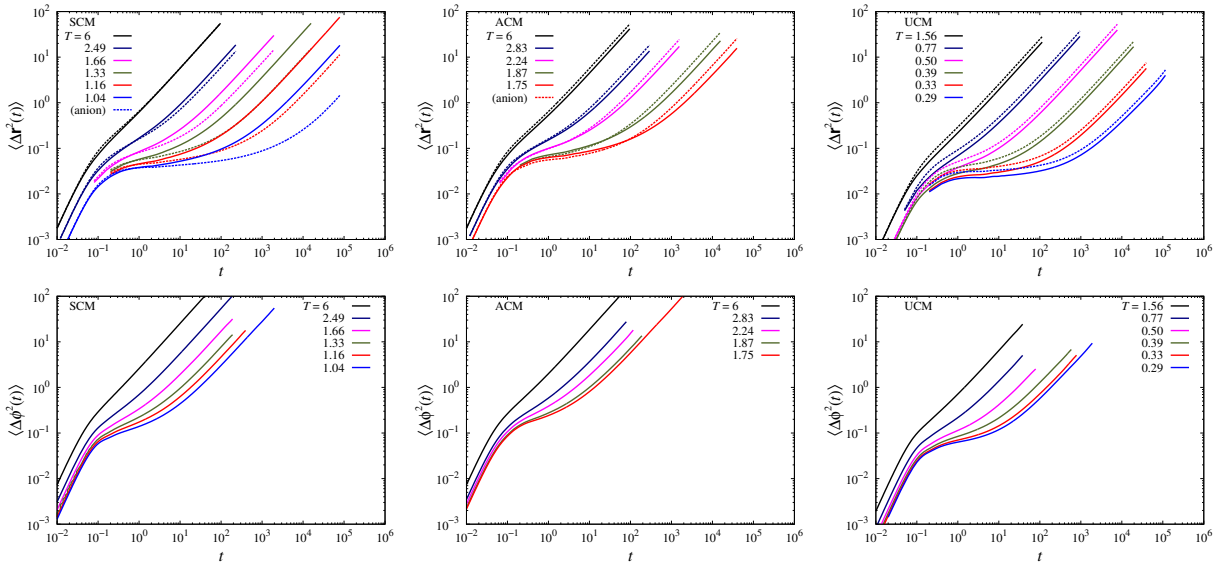

Fig. 5 Mean squared displacement of the constituents of SCM (left), ACM (center), and UCM (right), where the upper panels indicate translational motion for the cation (full line) and the anion (dashed line), and the bottom panels indicate rotational motion. In each panel temperature decreases from the upper to the lower graph. At low temperatures all the models show subdiffusive dynamics at the intermediate time scale, and this time regime becomes longer as the temperature decreases. The rotational motion shows less subdiffusivity than the translational motion at all models.

group of studies τ is used as the approximation for η, $D\tau/T$ thus becomes constant.[52] In the others η is approximated to be τ/T to make $D\tau$ constant.[11,29,30] Following the latter way, we look for the breakdown of the SE and the Debye-Stokes-Einstein (DSE) relations. When the dynamics of the system is well described by mean-field behavior, $F_s(q,t) = \exp[-q^2 Dt]$ and $C_l(t) = \exp[-l(l+1)D_R t]$, thus $q^2 D\tau_\alpha = 1$ and $l(l+1)D_R\tau_R^{(l)} = 1$.

Figs. 6(d)-(f) show the breakdown of the SE relation at low temperature. Dynamic heterogeneity induced by the correlated motion of mobile particles, or hierarchical nature of dynamics can explain this breakdown.[29,30] At $T \approx 2$ for IL models and $T \approx 0.6$ for UCM, the diffusion constants, D and D_R, and the relaxation times, τ_α and $\tau_R^{(2)}$, start decoupling with temperature decreasing. It is noticeable that the temperatures at which the diffusion constant and the relaxation time start to decouple fall into those where the subdiffusive regime starts to arise apparently.

This weak violation of the SE relation gives them the scaling exponent values between 0.75 and 0.9 at low temperature, via $D \sim \tau_\alpha^{-\zeta_D}$, and the values of ζ_D are shown in Fig. 6. At long length scale translational motion converges to the Fickian diffusion, which has been considered as homogeneous dynamics. The rotational diffusion, however, shows strong decoupling between D_R and $\tau_R^{(2)}$. While $\tau_R^{(2)}$ shows similar trend with τ_α (Figs. 4 and 6(a)), the rotational diffusion at low temperature does not become as slow as the translational one (Fig. 5). This trend has also been observed in other glassy systems made up of anisotropic molecules.[51,52] With this strong violation of the DSE relation, one might interpret the rotational motion is more dynamically heterogeneous than translational motion, but the dynamic heterogeneity measured by the four-point correlation function shows inconsistent evidence. We will discuss this in the next section.

3.3 Dynamic heterogeneity

We first briefly introduce the formalism of four-point correlation functions because dynamic heterogeneity has been widely studied in this frame work.[25,27,28,32,34–36,62] A four-point density correlation function detects the correlation between the dynamics at the different positions. Since the correlation function was originally coined for spin glass systems,[25,71] in order for it to be applicable in a continuous position space, correlation between $\rho(\mathbf{x}_0,t_0)$ and $\rho(\mathbf{x}_0,t_0+t)$ is coarse-grained with ξ_1: $\rho(\mathbf{x}_0+\mathbf{y},t_0)$ and $\rho(\mathbf{x}_0+\mathbf{y},t_0+t)$ with ξ_2,[25,35] where $\rho(\mathbf{x}',t')$ is the microscopic density at position $\mathbf{x}'$ and time t'. Thus, the four-point correlation function, $G_4(y,t;\xi_1,\xi_2)$, for the exact form of which we refer to previous studies,[25,27,28,34–36,62] correlates the dynamics of S_0 and S_x delineated in Fig. 7 with $t_1 - t_0 = \tau_1 = t$. The characteristic length scale of dynamic heterogeneity, ξ_{dh}, is obtained by varying y with the other parameters usually fixed at $\tau_1 = \tau_\alpha$, $\xi_1 = \xi_2 = 2\pi/k$.[35] We postpone discussion on the dynamic length scale until our next study and focus on the time scale.[72]

The time scale of the four-point correlation function is extracted from the four-point dynamic susceptibility, $\chi_4(k,t)$, which is the dynamic correlation between two regions inte-

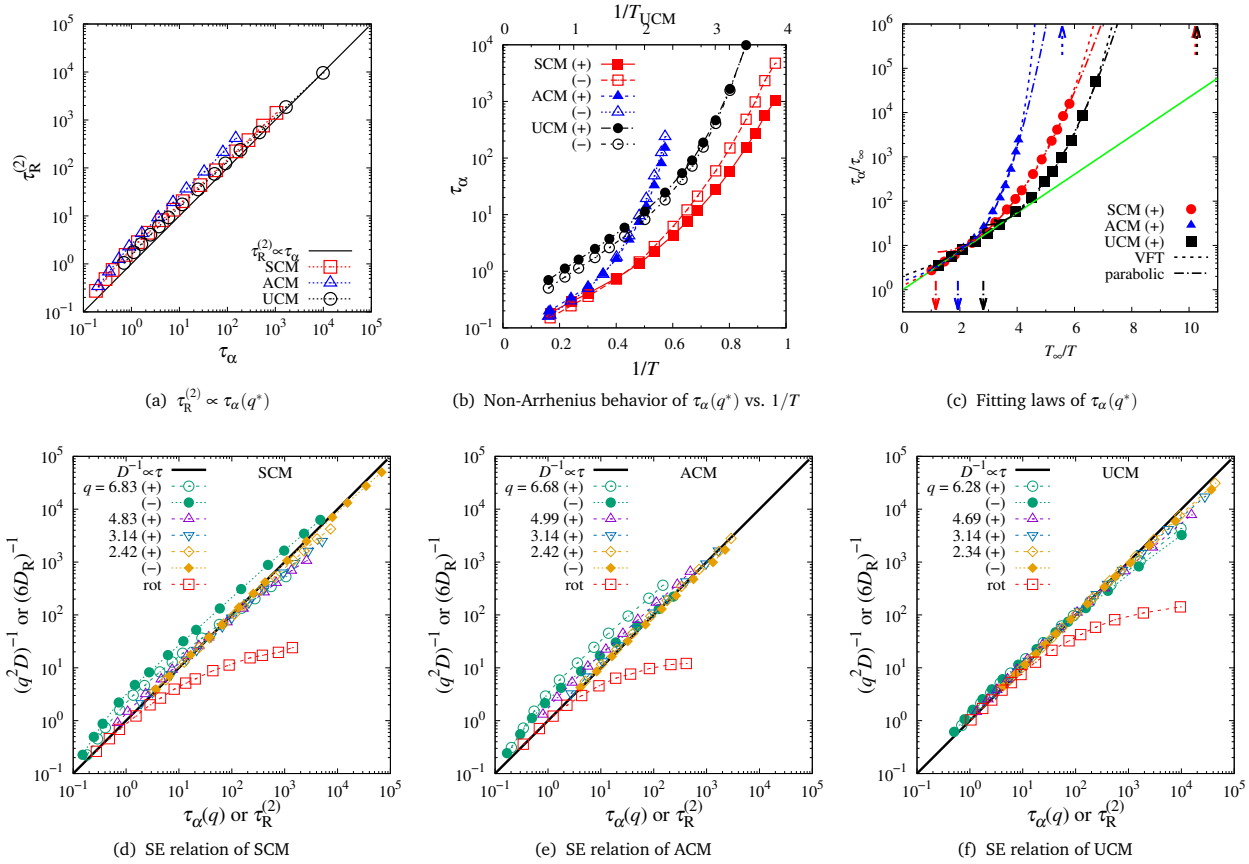

Fig. 6 (a) $\tau_R^{(2)}$ is scaled by $\tau_\alpha(q^*)$ very well: $\tau_R^{(2)} \propto \tau_\alpha^1$. The reorientational and the structural relaxation is very well coupled. (b) $\tau_\alpha(q^*)$ is plotted versus $1/T$. (+) and (-) respectively indicate the cation and the anion. The temperatures for UCM is indicated at the top scale. At low temperature, $T <$ 2.5, 3.6, and 0.6 for SCM, ACM, and UCM, respectively, all the models show non-Arrhenius behavior of the α-relaxation time, $\tau_\alpha(q^*)$, of the intermediate scattering functions. (c) At high temperature $\tau_\alpha(q^*)$ and T are fitted by the Arrhenius law, $\tau_\alpha = \tau_\infty \exp[T_\infty/T]$, where T_∞ = 6.1(6.7), 7.1(7.8), and 2.0(1.9) for cation(anion) of SCM, ACM, and UCM, respectively. ACM looks the most fragile. The arrows at the bottom indicate the onset temperature, T_o, for the parabola fitting, $\ln\tau \sim 1/T^2 - 1/T_o^2$, and the arrows at the top indicate the singular point, T_0, from the VFT fitting, $\ln\tau \sim 1/(T - T_0)$. (d)-(f) The scaling relation, $D \sim \tau_\alpha^{-\zeta_D}$, shows weak violation of the SE relation with the exponents, ζ_D between 0.75 and 0.9 at low temperature and at the short length scale, $q = q^*$. As the length scale becomes longer the SE relation recovers. D_R is much more decoupled from $\tau_R^{(2)}$ than the breakdown of the translational SE relation. q values are noted in the figure, and for brevity only the shortest and the longest length scales are indicated for the anion.

grated over all space of $\mathbf{y}$. Its explicit form,

$$\chi_4(k,t) = N\left\{ \left\langle \hat{F}_s(\mathbf{k},t_0,t_0+t)^2 \right\rangle - \left\langle \hat{F}_s(\mathbf{k},t_0,t_0+t) \right\rangle^2 \right\}, \qquad (9)$$

depicts the dynamic fluctuation of the two-point correlator, $\hat{F}_s(\mathbf{k},t_0,t_0+t)$. The characteristic time scale, t_4, of dynamic heterogeneity in this frame work is defined as the time at which the dynamic fluctuation is the maximum. It has been reported, however, to be proportional and similar to the time scale, τ_α, of a two-point density correlation function, *i.e.*, $t_4 \propto \tau_\alpha$,[27,28,72] and the models studied in this paper are no exceptions although the results are not shown here.

On the other hand, a three-time correlation function (3TCF), a four-point correlation function in time domain, defined analogously to the conventional four-point correlation function, $G_4(y,t;\xi_1,\xi_2)$, yields a time scale distinct from t_4. The dynamical correlation between different time windows is expressed as[39,43–47,58]

$$\begin{aligned}\widetilde{F}_4(\tau_1,t_w,\tau_2;\mathbf{k}_1,\mathbf{k}_2) &= \langle\hat{\rho}(-\mathbf{k}_1,t_0)\hat{\rho}(\mathbf{k}_1,t_1)\hat{\rho}(-\mathbf{k}_2,t_2)\hat{\rho}(\mathbf{k}_2,t_3)\rangle \\ &\quad - \langle\hat{\rho}(-\mathbf{k}_1,t_0)\hat{\rho}(\mathbf{k}_1,t_1)\rangle\langle\hat{\rho}(-\mathbf{k}_2,t_2)\hat{\rho}(\mathbf{k}_2,t_3)\rangle \\ &= \left\langle \hat{F}_s(\mathbf{k}_1,t_0,t_1)\hat{F}_s(\mathbf{k}_2,t_2,t_3)\right\rangle \\ &\quad - \left\langle \hat{F}_s(\mathbf{k}_1,t_0,t_1)\right\rangle\left\langle \hat{F}_s(\mathbf{k}_2,t_2,t_3)\right\rangle, \qquad (10)\end{aligned}$$

where the two-point correlator, $\hat{F}_s(\mathbf{k},t',t'')$, correlates between $\hat{\rho}(-\mathbf{k},t')$ and $\hat{\rho}(\mathbf{k},t'')$, and $\hat{\rho}(\mathbf{k},t)$ is the Fourier transform of the microscopic density. By adopting $\hat{F}_s(\mathbf{k},t',t'') = \frac{1}{N}\sum_j \cos[\mathbf{k}\cdot\Delta\mathbf{r}_j(t',t'')]$ as in Eq. (4) and setting the two length scales, $\mathbf{k}_1$ and

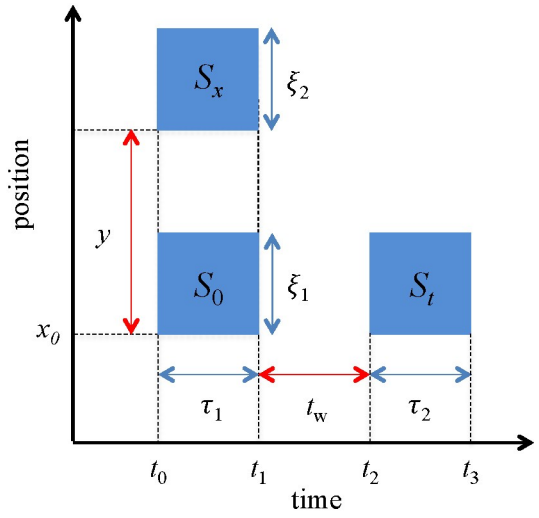

Fig. 7 Overview of four-point correlation functions. While G_4 correlates S_0 and S_x, F_4, defined analogously to G_4, does S_0 and S_t. $\tau_1 = t_1 - t_0$, $t_w = t_2 - t_1$, and $\tau_2 = t_3 - t_2$. By varying t_w, the dynamic heterogeneity time scale can be extracted from F_4.

$\mathbf{k}_2$, to be the same with $\mathbf{k}_1 = \mathbf{k}_2 = \mathbf{q}$, the first term of Eq. (10) becomes

$$\left\langle \frac{1}{N}\sum_{j=1}^{N} \cos\left[\mathbf{q}\cdot\Delta\mathbf{r}_j(t_0, t_0+\tau_1)\right] \right.$$
$$\left. \times \frac{1}{N}\sum_{l=1}^{N} \cos\left[\mathbf{q}\cdot\Delta\mathbf{r}_l(t_0+\tau_1+t_w, t_0+\tau_1+t_w+\tau_2)\right] \right\rangle, \quad (11)$$

and for brevity of this argument, we will consider the self part of Eq. (11), *i.e.*, $j = l$ of the summations. We thus define the 3TCF as[38,39,45–47,58]

$$F_4(\tau_1, t_w, \tau_2; q) = \left\langle \frac{1}{N}\sum_{j=1}^{N} \left\{ \cos\left[\mathbf{q}\cdot\Delta\mathbf{r}_j(t_0, t_0+\tau_1)\right] \right.\right.$$
$$\left.\left. \times \cos\left[\mathbf{q}\cdot\Delta\mathbf{r}_j(t_0+\tau_1+t_w, t_0+\tau_1+t_w+\tau_2)\right] \right\} \right\rangle, \quad (12)$$

which correlates the dynamics between the two time intervals, $(t_0, t_0+\tau_1)$ and $(t_0+\tau_1+t_w, t_0+\tau_1+t_w+\tau_2)$, or the dynamics of S_0 and S_t in Fig. 7. The characteristic time scale of F_4 is obtained by varying t_w with the parameters, τ_1, τ_2, and k fixed, similarly to the way $\xi_{\rm dh}$ is from G_4. The rotational form, $F_{4,\rm R}(\tau_1, t_w, \tau_2; l)$, of the 3TCF is defined straightforward by substituting $P_l(\hat{\mathbf{u}}_j(t'')\cdot\hat{\mathbf{u}}_j(t'))$ for $\cos[\mathbf{q}\cdot\Delta\mathbf{r}_j(t', t'')]$ in Eq. (12). While G_4 detects heterogeneous dynamics in different positions, thus is able to extract the length scale of dynamic heterogeneity, F_4 does in different times, thus, the time scale of dynamic heterogeneity. Although F_4 is defined analogously to G_4, it can be understood intuitively.

When the waiting time becomes greater, $t_w \to \infty$, the dynamics of the two time intervals are uncorrelated that $F_4(\tau_1, t_w, \tau_2; q)$ converges to $F_s(q, \tau_1)F_s(q, \tau_2)$, where a physical meaning of Eq. (12) can be derived. Given a dynamic fluctuation of particle j in a certain time duration τ_1, with the 3TCF we can figure out how long it must wait for the memory of this fluctuation to be lost. Here, the first part of Eq. (12) acts as a dynamic filter.[57] For faster particles $\cos\left[\mathbf{q}\cdot\Delta\mathbf{r}_j(t_0, t_0+\tau_1)\right]$, the first part of $F_4(\tau_1, t_w, \tau_2; q)$, has smaller values, but for very slow particles the cosine value is close to one. Slower particles have more contribution on $F_4(\tau_1, t_w, \tau_2; q)$, so the dynamic filter selects subpopulations of particles moving slower.

After dynamically filtering slow particles, it quantifies how fast the subpopulations recover to the average dynamics. The time scale of dynamic heterogeneity is the lifetime of the correlation function,[39,47]

$$\Delta F_4(t_w; q, \tau_1, \tau_2) = \frac{F_4(\tau_1, t_w, \tau_2; q) - F_s(q, \tau_1)F_s(q, \tau_2)}{F_4(\tau_1, 0, \tau_2; q) - F_s(q, \tau_1)F_s(q, \tau_2)}, \quad (13)$$

and from this we can focus on the dependence of dynamic heterogeneity on t_w. The value of $\Delta F_4(t_w)$ indicates how much dynamically heterogeneous the system is, and the time scale at which the $\Delta F_4(t_w)$ goes to zero is that of dynamic heterogeneity.

The waiting time is an important variable to quantify the correlation between the dynamics at the two time intervals. It is required to fix some of the parameters, q, τ_1, and τ_2 before studying the dependence of the 3TCF on the waiting time. It is obvious to set $\tau_1 = \tau_2 = \tau_\alpha$ since the dynamic heterogeneity is observed to be more prominent at time scale close to $\tau_\alpha \approx t_4$. We, then, fix the length scale with four different q values indicated in Fig. 8 from q^* to $q_0/2$. The lifetime of ΔF_4, $\tau_{\rm dh}(q)$, is defined such that $\Delta F_4(t_w = \tau_{\rm dh}; q, \tau_\alpha, \tau_\alpha) = e^{-1}$, and its rotational form, $\tau_{\rm dh,R}$, such that $\Delta F_{4,\rm R}(t_w = \tau_{\rm dh,R}; l = 2, \tau_{\rm R}^{(2)}, \tau_{\rm R}^{(2)}) = e^{-1}$, where $\Delta F_{4,\rm R}(t_w; l, \tau_1, \tau_2)$ is defined by replacing $F_4(\tau_1, t_w, \tau_2; q)$ and $F_s(q, \tau')$ with $F_{4,\rm R}(\tau_1, t_w, \tau_2; l)$ and $C_l(\tau')$, repectively.

Previous studies have calculated for $\tau_{\rm dh}$ from a differently defined correlation function, $\Delta(t_w)$, by integrating $F_4(\tau_1, t_w, \tau_2; q)$ over τ_2,[31,46]

$$\Delta(t_w; q, \tau_1) = \int_0^\infty d\tau_2 \left[\frac{F_4(\tau_1, t_w, \tau_2; q)}{F_s(q, \tau_1)} - F_s(q, \tau_2)\right], \quad (14)$$

which measures the difference between the filtered dynamics and the bulk dynamics. The time scale of dynamic heterogeneity, $\tau_{\rm dh}^{(\Delta)}$, from Eq. (14) is defined as $\Delta(t_w = \tau_{\rm dh}^{(\Delta)})/\Delta(0) = 1/e$. An otherwise defined time scale of dynamic heterogeneity has been employed in other studies.[38,45] One can replace $\Delta(\tau_{\rm dh}^{(\Delta)})/\Delta(0)$ with the one obtained by integrating the 3TCF over both τ_1 and τ_2.[38,45] We check in the insets of Fig. 8 the consistency between the two time scales, $\tau_{\rm dh}^{(\Delta)} \propto \tau_{\rm dh}$, and we expect that the time scales in Refs. [38,45] will show the same relation. Rotational motion shows a little discrepancy at ACM, but it is ascribed to the statistical error of $\tau_{\rm dh}^{(\Delta)}$ since it needs longer trajectories to integrate. We, therefore, choose $\tau_{\rm dh}$ for the characteristic time scale of dynamic heterogeneity in further discussion.

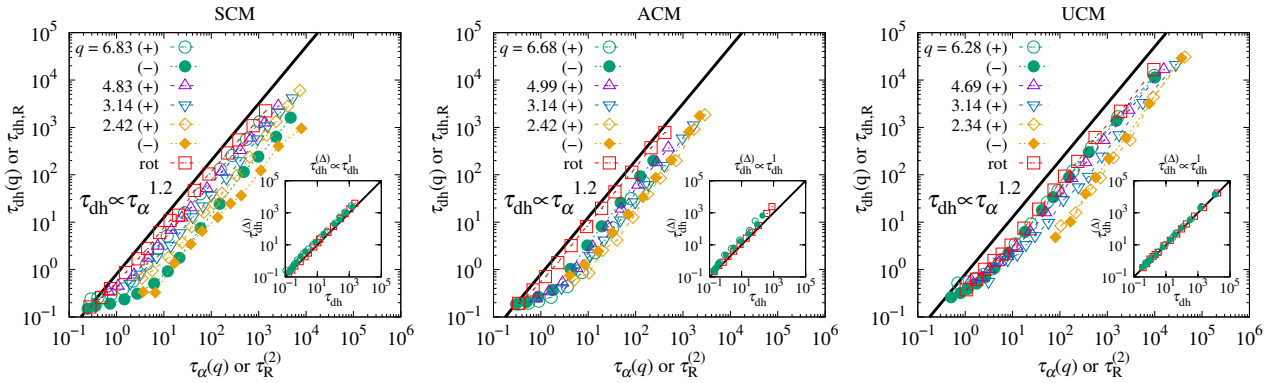

Fig. 8 τ_{dh} can be scaled by τ_α through the scaling relation $\tau_{dh} \propto \tau_\alpha^{\zeta_{dh}}$, where all the systems (left: SCM, center:ACM, right: UCM) have similar scaling exponent, $\zeta_{dh} \approx 1.2$. The solid line is a guide. For the anions, only the longest and the shortest length scale are plotted for brevity, but the trend is the same as for the cations. (Insets) $\tau_{dh}^{(\Delta)} \propto \tau_{dh}$ at all systems with $q = q^*$ except at the lowest temperature of ACM showing a little discrepancy. It is ascribed to the statistical error of $\tau_{dh}^{(\Delta)}$ since it needs longer trajectories to integrate (see Eq. (14)).

Consequently, the relation between τ_{dh} and τ_α, is obtained in Fig. 8. From the results of D and the τ_α ACM shows slower dynamics, leading us to expect that τ_{dh} of ACM will be greater than that of SCM and UCM, thus greater dynamic heterogeneity. When the models are compared at the same temperatures, it seems as if charge induced the dynamic heterogeneity and as if asymmetry in charge distribution strengthened it.[3] τ_{dh}, however, can be scaled by τ_α through the scaling relation $\tau_{dh} \propto \tau_\alpha^{\zeta_{dh}}$, where $\zeta_{dh} \approx 1.2$ in all the systems: ACM at the shortest length scale, $q = q^*$, may seem an exception with a bit greater value, but it converges to ≈ 1.2 at longer length scales.

It is noteworthy that UCM is another kind of 50/50 binary mixture glass-forming liquids, some of which have been widely used as model systems[29,38,39,47,73] to study glassy dynamics. The most distinctive feature of UCM from the others is that the cation is made up of two components. As other binary mixture models UCM shows heterogeneous dynamics, and its heterogeneity does not change by assigning charges into its component because the dynamics of both SCM and ACM are not much different from that of the uncharged counterpart, UCM, if the temperatures are rescaled (see Figs. 6(b)-(c)), and all the models have the same exponent, ζ_{dh}. It was reported that the time scales of dynamic heterogeneity have different scaling behavior with respect to τ_α when the types of short-range interaction differ.[38] Since the short-range interaction and the structure of the models in this paper are the same, we believe that dynamic properties are not affected by the long range interaction, but rather by the molecular structure, which are determined by short range interaction. This result is consistent to the previous study on a coarse-grained IL model, where it was found that the work to individual ions is exerted primarily by the short-ranged LJ force, and thus argued that the dynamics is dominantly influenced by the LJ interaction.[11]

The time scale of dynamic heterogeneity of other glass forming liquids are worth while to be compared. As atomistic models, binary mixture systems show similar scaling behavior. Among them Ref. [38], where the 3TCF similar to that in this paper was employed, is generally in agreement with the present study. It was manifested that the fragile liquids have greater values of ζ_{dh} than the strong liquid, *e.g.* $\zeta_{dh} \approx 1.9$, 1.25, and 1.5 for the fragile liquids: Wahnström,[73] Kob-Andersen,[74] and the soft sphere models,[75] respectively, while a strong liquid model[76] mimicking SiO_2 shows $\zeta_{dh} \approx 0.9$. Another study with the soft sphere model found the exponent ≈ 1.08 using a 3TCF with a correlator different from the one used in the present paper.[47] This power-law relation is a general phenomenon in all the above models including the three models studied in this paper. The scaling relation is also comparable to that of KCMs, spin models for supercooled liquids. According to the study in Ref. [46], for both strong and fragile models $\zeta_{dh} \approx 1$, where they showed that a fragile system displays slightly more heterogeneous dynamics: 1.06 for the fragile liquid and 0.98 for the

Table 1 Comparison of the exponent, ζ_{dh}, values with other models ($\tau_{dh} \propto \tau_\alpha^{\zeta_{dh}}$)

Models	IL/UCM[b]	Wahn[c]	KA[c]	SS[c]	SS[d]	NTW[c]	KCM[e]
ζ_{dh}	1.2	1.9	1.25	1.5	1.08	0.9	≈ 1[e]

[b] IL models include SCM and ACM. All the models studied in this paper have the same exponent.
[c] Ref. [38]. KA: Kob-Andersen 80/20 LJ binary mixture, Wahn: Wahnström 50/50 LJ binary mixture, SS: Soft sphere 50/50 soft core binary mixture, NTW: tetrahedral network-forming 1:2 mixture
[d] Ref. [47]. SS: the same model as SS in Ref. [38] with τ_{dh} calculated from a different correlator
[e] Ref. [46]. $\zeta_{dh} = 1.06$ for the East model, a KCM for a fragile liquid, and 0.98 for the FA model for a strong liquid.

strong liquid, but the exponents do not show as much difference in fragility as in atomistic models. The exponent values are summarized in Table 1.

Now, it seems appropriate to note an interesting finding that the length scale of structural relaxation is reflected very little by the dynamic heterogeneity, in contrast to the breakdown of the SE relation (see Fig. 8 and Figs. 6(d)-(f)). As the length scale increases, the ISFs become exponential and the diffusion and the structural relaxation are coupled. From this perspective it should follow the dynamics of Brownian motion at a long length scale. Time scale of dynamic heterogeneity studied in this paper, however, maintains the same exponent regardless of the length scale. It persuades us to believe that the dynamics is Fickian at the long length scale but still heterogeneous although we did not capture a tangible evidence as in Ref. [60]. It is obvious that $\tau_{\rm dh}$ is a characteristic time scale of dynamic heterogeneity that is distinguished from the two-point time scales, τ_α and $\tau_{\rm R}^{(2)}$.

Moreover, in the perspective of dynamic heterogeneity time scale, it is also notable that translational and rotational motions are strongly coupled, both having the same exponent, $\zeta_{\rm dh}$, despite the strong decoupling in diffusion between the two motions (see Fig. 8 and Figs. 6(d)-(f)). For the discussion on this we employ a previous study on supercooled model system with dumbbell molecules,[51] where the authors ascribed this inconsistency to the inadequacy of the definition, Eq. (8). They found that $\langle \Delta\boldsymbol{\phi}^2(t)\rangle$ increases diffusively even when the orientation of the molecule is actually trapped and doing librational motion. This leads decoupling between $D_{\rm R}$ and D with the former increasing further. It needs in-depth investigation to tell if this interesting discrepancy comes from real physics or contribution from the librational motion in rotational dynamics. Nevertheless, we used this definition because there is no other way, at the present, of calculating angular displacement unboundedly. If the librational motion were possible to be expressed in a proper way, excluding the librational motion from stacking fallaciously to increase MSAD continuously, the breakdown of the DSE relation would not be that severe.[f]

4 Conclusions

We investigated how the charge distribution on ions and the length scale of the structural relaxation effects the dynamic properties and the dynamic heterogeneity of IL systems by performing the molecular dynamics simulations on two simple models of ILs and their neutral counterpart: symmetric-charge model (SCM), asymmetric-charge model (ACM), and uncharged model (UCM). We found that all the models maintain amorphous liquid structures, and they show nonexponential relaxation and subdiffusive behavior at low temperatures.

Coulomb interaction lowers the temperature at which glassy dynamics appears, and the asymmetry in charge distribution provokes the time scale of dynamics longer. SCM shows similar dynamic properties of typical ILs in that the cation shows faster process than the anion in both structural relaxation and diffusion. Relations between τ_α and temperature show that all models behaves like fragile liquids. The SE relation breaks down at short length scales, and it recovers as the length scale increases. The rotational motion, however, shows strong decoupling between the diffusion and the relaxation time: strong breakdown of the DSE relation.

We correlated a four-point correlation function to its two-point correlation function by adopting the 3TCF, analogously to the conventional four-point correlation function. The lifetime, $\tau_{\rm dh}$, of dynamic heterogeneity defined from the 3TCF, scales very well with the time scale, τ_α, of the two-point correlation function: $\tau_{\rm dh} \propto \tau_\alpha^{\zeta_{\rm dh}}$ with $\zeta_{\rm dh} \approx 1.2$, which holds for both the translational and the rotational correlation functions with the same exponent. This power-law relation is a general phenomenon in glass-forming liquids, similar to the relation between $\xi_{\rm dh}$ and τ_α, although the exponent is dependent on the models from other studies: fragile liquids have greater values than strong liquids. The rotational dynamics also shows the same dynamic heterogeneity giving the same $\zeta_{\rm dh}$ value as the translational one despite the strong breakdown of DSE relation. It is apparent that the time scale of dynamic heterogeneity is a distinctive time scale from the two-point correlation functions, such as the structural relaxation and the rotational relaxation.

The exponent, $\zeta_{\rm dh}$, is irrelevant to the charge distribution on the molecule, type of interactions, and even the length scales of the two-point correlation function. With the longer length scale the structural relaxation is detected, the more it becomes Fickian while the dynamics is seemingly maintaining its heterogeneity. We expect that our results provide useful insight on the relation between the dynamic heterogeneity and the types of molecular interaction although the 3TCFs need more theoretical supports compared to the conventional four-point correlation function. The length scale and other properties of dynamic heterogeneity of these models are to be obtained in our further study.[72]

[f] A brief speculation on this is included in the ESI, related to the dependence the time interval on MSAD.

Acknowledgements

The authors thank Daun Jeong, Kang Kim, Ryoich Yamamoto, and Grzegorz Szamel for helpful discussions and comments. This work was supported by the National Research Foundation of Korea (NRF) grants funded by the Korea government (Nos. 2007-0056095 and 2012R1A1A2042062), the Ministry of Education, Science and Technology, subjected to the project EDISON (EDucation-research Integration through Simulation On the Net, Grant No. 2012M3C1A6051724), and the Brain Korea (BK) 21 Plus program.

References

1 H. Weingärtner, *Angew. Chem. Int. Ed.*, 2008, **47**, 654–670.
2 H. Shirota and E. W. Castner, *J. Phys. Chem. A*, 2005, **109**, 9388–9392.

3 D. Roy, N. Patel, S. Conte and M. Maroncelli, *J. Phys. Chem. B*, 2010, **114**, 8410–8424.

4 H. Tokuda, K. Ishii, M. A. B. H. Susan, S. Tsuzuki, K. Hayamizu and M. Watanabe, *J. Phys. Chem. B*, 2006, **110**, 2833–2839.

5 M. N. Kobrak and N. Sandalow, Molten Salts XIV, Pennington, NJ, 2006, pp. 417–425.

6 H. V. Spohr and G. N. Patey, *J. Chem. Phys.*, 2009, **130**, 104506.

7 M. Malvaldi and C. Chiappe, *J. Phys.: Condens. Matter*, 2008, **20**, 035108.

8 D. Roy and M. Maroncelli, *J. Phys. Chem. B*, 2010, **114**, 12629–12631.

9 Y. Shim, J. Duan, M. Y. Choi and H. J. Kim, *J. Chem. Phys.*, 2003, **119**, 6411.

10 Y. Shim and H. J. Kim, *J. Phys. Chem. B*, 2008, **112**, 11028–11038.

11 D. Jeong, M. Y. Choi, H. J. Kim and Y. Jung, *Phys. Chem. Chem. Phys.*, 2010, **12**, 2001–2010.

12 D. Jeong, D. Kim, M. Y. Choi, H. J. Kim and Y. Jung, *Ionic Liquids: Theory, Properties, New Approaches*, InTech, 2011, pp. 167–182.

13 D. Kim, D. Jeong and Y. Jung, *Phys. Chem. Chem. Phys.*, 2014, **16**, 19712–19719.

14 D. Jeong, M. Y. Choi, Y. Jung and H. J. Kim, *J. Chem. Phys.*, 2008, **128**, 174504.

15 T. Pal and R. Biswas, *J. Chem. Phys.*, 2014, **141**, 104501.

16 C. J. Margulis, H. A. Stern and B. J. Berne, *J. Phys. Chem. B*, 2002, **106**, 12017–12021.

17 M. G. D. Pópolo and G. A. Voth, *J. Phys. Chem. B*, 2004, **108**, 1744–1752.

18 Z. Hu and C. J. Margulis, *Proc. Natl. Acad. Sci. U.S.A.*, 2006, **103**, 831–836.

19 J. Habasaki and K. L. Ngai, *J. Chem. Phys.*, 2008, **129**, 194501.

20 B. L. Bhargava and S. Balasubramanian, *J. Chem. Phys.*, 2005, **123**, 144505.

21 S. M. Urahata and M. C. C. Ribeiro, *J. Chem. Phys.*, 2005, **122**, 024511.

22 T. I. Morrow and E. J. Maginn, *J. Phys. Chem. B*, 2002, **106**, 12807–12813.

23 A. Triolo, O. Russina, V. Arrighi, F. Juranyi, S. Janssen and C. M. Gordon, *J. Chem. Phys.*, 2003, **119**, 8549.

24 D. Chakrabarty, D. Seth, A. Chakraborty and N. Sarkar, *J. Phys. Chem. B*, 2005, **109**, 5753–5758.

25 L. Berthier and G. Biroli, *Rev. Mod. Phys.*, 2011, **83**, 587.

26 M. T. Cicerone and M. D. Ediger, *J. Chem. Phys.*, 1996, **104**, 7210.

27 G. Szamel and E. Flenner, *Phys. Rev. E*, 2006, **74**, 021507.

28 G. Szamel and E. Flenner, *Phys. Rev. E*, 2010, **81**, 031507.

29 L. O. Hedges, L. Maibaum, D. Chandler and J. P. Garrahan, *J. Chem. Phys.*, 2007, **127**, 211101.

30 Y. Jung, J. P. Garrahan and D. Chandler, *Phys. Rev. E*, 2004, **69**, 061205.

31 Y. Jung, J. P. Garrahan and D. Chandler, *J. Chem. Phys.*, 2005, **123**, 084509.

32 S.-W. Choi, S. Kim and Y. Jung, *J. Chem. Phys.*, 2015, **142**, 244506.

33 L. Berthier and R. L. Jack, *Phys. Rev. E*, 2007, **76**, 041509.

34 S. C. Glotzer, V. N. Novikov and T. B. Schrøder, *J. Chem. Phys.*, 2000, **112**, 509–512.

35 N. Lacevic, F. Starr, T. Schroder and S. Glotzer, *J. Chem. Phys.*, 2003, **119**, 7372–7387.

36 E. Flenner and G. Szamel, *Phys. Rev. Lett.*, 2010, **105**, 217801.

37 E. Flenner and G. Szamel, *Nature Phys.*, 2012, **8**, 696–697.

38 K. Kim and S. Saito, *J. Chem. Phys.*, 2013, **138**, 12A506.

39 H. Mizuno and R. Yamamoto, *Phys. Rev. E*, 2011, **84**, 011506.

40 M. T. Cicerone and M. D. Ediger, *J. Chem. Phys.*, 1995, **103**, 5684.

41 C.-Y. Wang and M. D. Ediger, *J. Phys. Chem. B*, 1999, **103**, 4177–4184.

42 M. D. Ediger, *Annu. Rev. Phys. Chem.*, 2000, **51**, 99–128.

43 E. Flenner and G. Szamel, *Phys. Rev. E*, 2004, **70**, 052501.

44 K. Kim and S. Saito, *Phys. Rev. E*, 2009, **79**, 060501.

45 K. Kim and S. Saito, *J. Chem. Phys.*, 2010, **133**, 044511.

46 S. Léonard and L. Berthier, *J. Phys.: Condens. Matter*, 2005, **17**, S3571–S3577.

47 H. Mizuno and R. Yamamoto, *Phys. Rev. E*, 2010, **82**, 030501(R).

48 S. A. Mackowiak, L. M. Leone and L. J. Kaufman, *Phys. Chem. Chem. Phys.*, 2011, **13**, 1786–1799.

49 S. Karmakar, C. Dasgupta and S. Sastry, *Proc. Natl. Acad. Sci. U.S.A.*, 2009, **106**, 3675–3679.

50 S. Kämmerer, W. Kob and R. Schilling, *Phys. Rev. E*, 1997, **56**, 5450–5461.

51 S.-H. Chong and W. Kob, *Phys. Rev. Lett.*, 2009, **102**, 025702.

52 M. G. Mazza, N. Giovambattista, H. E. Stanley and F. W. Starr, *Phys. Rev. E*, 2007, **76**, 031203.

53 B. Doliwa and A. Heuer, *Phys. Rev. Lett.*, 1998, **80**, 4915–4918.

54 J. Qian, R. Hentschke and A. Heuer, *J. Chem. Phys.*, 1999, **110**, 4514–4522.

55 K. Schmidt-Rohr and H. W. Spiess, *Phys. Rev. Lett.*, 1991, **66**, 3020–3023.

56 A. Heuer, M. Wilhelm, H. Zimmermann and H. W. Spiess, *Phys. Rev. Lett.*, 1995, **75**, 2851–2854.

57 A. Heuer, *Phys. Rev. E*, 1997, **56**, 730.

58 A. Heuer and K. Okun, *J. Chem. Phys.*, 1997, **106**, 6176.

59 R. Yamamoto and A. Onuki, *Phys. Rev. E*, 1998, **58**, 3515.

60 J. Kim, C. Kim and B. J. Sung, *Phys. Rev. Lett.*, 2013, **110**, 047801.

61 K. V. Edmond, M. T. Elsesser, G. L. Hunter, D. J. Pine and E. R. Weeks, *Proc. Natl. Acad. Sci. U.S.A.*, 2012, **109**, 17891–17896.
62 C. Dasgupta, A. V. Indrani, S. Ramaswamy and M. K. Phani, *Europhys. Lett.*, 1991, **15**, 307.
63 Y. Wang and G. A. Voth, *J. Am. Chem. Soc.*, 2005, **127**, 12192–12193.
64 S. Pronk, S. Páll, R. Schulz, P. Larsson, P. Bjelkmar, R. Apostolov, M. R. Shirts, J. C. Smith, P. M. Kasson, D. van der Spoel, B. Hess and E. Lindahl, *Bioinformatics*, 2013, **29**, 845–854.
65 J. D. Weeks, D. Chandler and H. C. Andersen, *J. Chem. Phys.*, 1971, **54**, 5237.
66 J. N. Canongia Lopes, J. Deschamps and A. A. H. Pádua, *J. Phys. Chem. B*, 2004, **108**, 2038–2047.
67 K. Mitsuhiro, K. R. Harris, N. Tsuchihashi, K. Ibuki and M. Ueno, *J. Phys. Chem. B*, 2007, **111**, 2062–2069.
68 Y. S. Elmatad, D. Chandler and J. P. Garrahan, *J. Phys. Chem. B*, 2009, **113**, 5563–5567.
69 Y. S. Elmatad, D. Chandler and J. P. Garrahan, *J. Phys. Chem. B*, 2010, **114**, 17113–17119.
70 M. P. Allen and D. J. Tilesley, *Computer Simulation of Liquids*, Clarendon, Oxford, 1987.
71 S. F. Edwards and P. W. Anderson, *J. Phys. F: Metal Phys.*, 1975, **5**, 965–974.
72 S. Kim, S.-W. Park and Y. Jung, (in preparation).
73 G. Wahnström, *Phys. Rev. A*, 1991, **44**, 3752–3764.
74 W. Kob and H. C. Andersen, *Phys. Rev. E*, 1995, **51**, 4626.
75 B. Bernu, Y. Hiwatari and J. P. Hansen, *J. Phys. C: Solid State Phys.*, 1985, **18**, L371–L376.
76 D. Coslovich and G. Pastore, *J. Phys.: Condens. Matter*, 2009, **21**, 285107.